Academic Journal of Science and Technology
ISSN: 2771-3032 | Vol. 19, No. 1, 2026

Vibration Suppression of Integrated Joint Servo System for Robots Based on Fuzzy Adaptive PID

Xiuwen Shan [1], Lixiang Sun [1], Yi Zhang [2], Hanpei Wei [2, *]

[1] Joint Technology Transfer Center of Yancheng Polytechnic College, Yancheng Polytechnic College, Yancheng, Jiangsu, 224005, China
[2] School of Automation, Jiangsu University of Science and Technology, Zhenjiang, Jiangsu, 212003, China

[*] **Corresponding author**: Hanpei Wei (Email: 1506089882@qq.com)

Abstract: Due to the limitation of working environment, the underground power grid detection robot needs to ensure a very low failure rate. The vibration of the robot will lead to poor positioning accuracy and short service life of core components. Considering that the robot is a multi-variable and multi-coupling nonlinear system, its vibration is mainly reflected in the speed fluctuation of the robot servo motor. The change of the working attitude and position of the robot will lead to the sudden change of torque and moment of inertia, which is not conducive to the smoothness of speed control. In order to solve this problem, this paper studies the intelligent integrated joint of robot, investigates the mechanism of robot vibration, proposes the intelligent control strategy of fuzzy adaptive PID control, suppresses the vibration of integrated joint servo system, and compares it with the traditional control strategy. Through the robot dynamic model, the moment of inertia of the robot is calculated online in real time, which is given as the input of the intelligent joint. The experimental research is carried out with the underground power grid detection robot as the test platform, which proves the practicability and effectiveness of the method proposed in this paper.

Keywords: Intelligent Integrated Joint; Fuzzy Adaptive PID; Vibration Suppression.

1. Introduction

Robots are widely used in various industries, freeing humans from heavy, dangerous, and harsh working environments. With the further development of computer technology, artificial intelligence technology, sensing technology, and control technology, the robotics industry will enter a fast lane of development. Currently, multiple fields have raised higher requirements for robots in terms of fault tolerance, response speed, adaptive and self-learning capabilities, and control accuracy. In addition, the working environment, control process, and control objects of robots have become increasingly complex, often exhibiting complex uncertainties and nonlinearities such as unknown parameters, external disturbances, and structural uncertainties, which make it impossible to accurately establish mathematical models. Sun et al. studied the directional stiffness and natural frequency distribution of robots and analyzed the vibration results based on different operating conditions of robots [1]. Kim and Croft proposed three methods: optimal s-curve trajectory, robust zero-vibration shaper, and dynamic zero-vibration shaper, to suppress multimodal vibrations of flexible joint robots under computational torque control based on rigid models [2]. Elvira et al. also achieved certain motion estimation effects by using Kalman filtering to fuse accelerometer and gyroscope sensing data to suppress joint vibrations [3]. In practical applications, the current research on vibration suppression by domestic robot manufacturers focuses on the design of notch filters: that is, avoiding certain vibration points by designing notch filters. Although notch filters can quickly suppress vibrations at certain frequency points, they cannot solve the problem when robots exhibit broadband vibrations [4, 5]. Experimental results show that when notch filters are turned on, the operating noise of the robot increases, and changes in the load inertia of the robot often lead to frequency drift phenomena [6]. Notch filters cannot solve the frequency drift vibration problem under varying inertia conditions. To address issues such as varying inertia, varying frequency, and broadband vibrations of robots, and to overcome the shortcomings of notch filters, this paper proposes a fuzzy adaptive proportional-integral-derivative (PID) control intelligent control strategy to further improve the working life and control accuracy of the robot control system, and to enhance the steady-state performance of the control system [7].

2. Proposal of the Problem

2.1. Mobile Intelligent Robot for Underground Power Grid

Servo motors, as the power system of robots, are connected to harmonic reducers, forming the robot's actuator. The accuracy and lifespan of this actuator determine the accuracy and lifespan of the robot body.

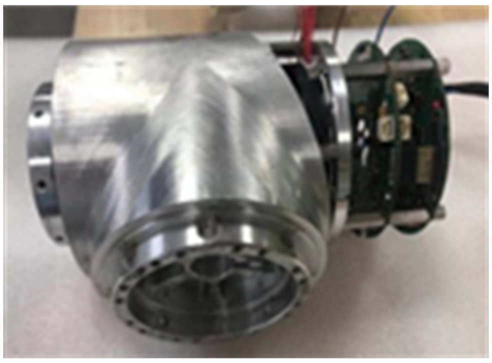

Figure 1. Integrated intelligent joint structure for robots

Traditional robots are composed of controllers, harmonic reducers, servo motors, and servo drivers, which are bulky and costly. By adopting intelligent robot joints that are integrated and lightweight, the workload of robot assembly can be effectively reduced, and manufacturing costs can be lowered. Intelligent robots integrate harmonic reducers, servo motors, and servo drivers. Figure 1 shows the actual intelligent robot joint, with the motor + reducer part on the left and the servo driver on the right. It is powered by a DC 48V battery, and the servo driver outputs a three-phase sine wave AC voltage ranging from 0 to 33.9V, with an output voltage frequency range of 0 to 1000Hz.

Figure 2 shows the underground grid detection robot, which has four degrees of freedom, consisting of two 20-model intelligent joints and two 14-model intelligent joints. It is powered by a DC 48V battery with a capacity of 1kVA. The robot is equipped with a 2kg camera at the end for taking photos and detection. When the robot is in patrol mode, its arms are folded. When taking photos, the entire robotic arm is extended, with an arm span of 1.1 meters.

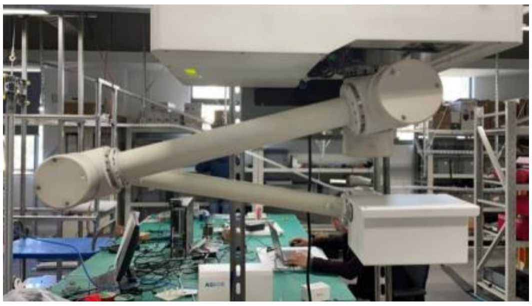

Figure 2. Underground power grid detection robot

The characteristics of this robot are:

1. Lightweight: The entire robot weighs no more than 10kg.

2. Low power consumption: In a stationary position, the total power consumption of the four joints is 30W. During arm movement, the instantaneous maximum current is 3A, and the arm extension time is 4 seconds.

3. Long arm extension: To meet the requirements for photography, the total length of the robotic arm has been extended from the standard 0.8 meters to 1.1 meters.

2.2. Issues Arising from Long-Endurance and Lightweight Mobile Robots

Mobile robots are a key development direction in the field of robotics. They require robots to be as lightweight as possible, but lightweight design can lead to the selection of undersized motors and reducers, resulting in reduced rigidity of the robotic arm. Since mobile robots need to extend their arm length during operation, this also brings about drastic changes in rotational inertia. When the robot transitions from its folded state to its photographing state, the arm length needs to be increased, causing the rotational inertia to change by more than eight times. Traditional speed loop regulators cannot meet the requirements of such significant changes in rotational inertia, leading to unstable rotational speed during movement and vibration in the robot. To address this issue, there are two solutions:

1. Increasing the rated torque of the motor and the rotational inertia of the motor rotor can reduce vibration, but it will result in an increase in the volume and weight of the joint module, leading to higher power consumption of the robot, shorter cruising time, and limited patrol space.

2. Design a new controller to meet the robot control requirements under large changes in rotational inertia and suppress vibration. This is also the key issue studied in this paper.

The vibration problem is one of the key core issues of robots and also the most challenging problem faced in robot research. Due to vibration, the lifespan of reducer components is shortened, and the accuracy of the robot is deteriorated. Tests have shown that when the instantaneous speed fluctuation of the servo motor exceeds plus or minus 8 rpm, vibration will significantly increase. Suppressing the speed fluctuation of the servo motor is the control idea of this article.

The intelligent integrated joint adopts a vector control system with three closed-loop controls: position, speed, and current. The position loop receives position commands from the host computer and compares them with the actual position of the motor to generate a speed signal. Currently, the position loop regulator mainly consists of a combination of proportional control and feedforward control. The speed command passes through the speed loop regulator to form a speed command. According to vibration meter data, if the instantaneous speed fluctuation of the robot joint can be controlled to be within ±6 rpm, vibration can be effectively suppressed.

During the robot's operation, continuous changes in its posture and load result in continuous variations in its moment of inertia. However, in traditional vector control systems for AC motors, only the motor's torque current and motor position are collected as control signal inputs. This paper combines a robot dynamics model to calculate the robot's real-time moment of inertia in real-time, and then employs a fuzzy intelligent PID control strategy to suppress the vibration of the robot body.

How to identify the moment of inertia of the load in real time is the difficulty and key point of this article.

3. Identification of Rotational Inertia based on Dynamics

3.1. Motion Model of Underground Exploration Robot

Based on the mechanical characteristics of the underground exploration robot and the electrical properties of each joint, the D-H parameters of the robotic arm are obtained as shown in Table 1, and the relevant dynamic parameters of the current robot are presented in Table 2.

After studying the kinematic model of the robotic arm, simulation experiments are required before applying the method to engineering experiments. Through simulation experiments, the running time of the algorithm processing can be verified.

Table 1. Robot arm D-H parameters

link	θ (rad)	d_i (mm)	a_i (mm)	α_i (rad)
1	0	0	0	0
2	π/2	±155	0	π/2
3	0	0	500	0
4	0	-136.5	500	0

Table 2. Relevant parameters of robotic arm dynamics

Parameter	Motor			
	No.1	No.2	No.3	No.4
Motor torque (Nm)	1.5	1.5	1.5	0.735
Mass (kg)	2.8	2.8	2.8	1.5
Angular velocity (°/s)	180	180	180	180
Reduction ratio	101	101	101	101

It is worth noting that the last column of Table 2 shows the reduction ratio of the current reduction mechanism. The output torque of the joint is equal to the motor output torque multiplied by the reduction ratio. During the mechanical design and hardware selection and configuration process, joints 1, 2, and 3 were designed using the same parameters. In addition, the inertia tensor matrix and center of mass position of each joint link required for dynamics were extracted from the mechanical design software.

3.2. Design of Robot Dynamics Controller

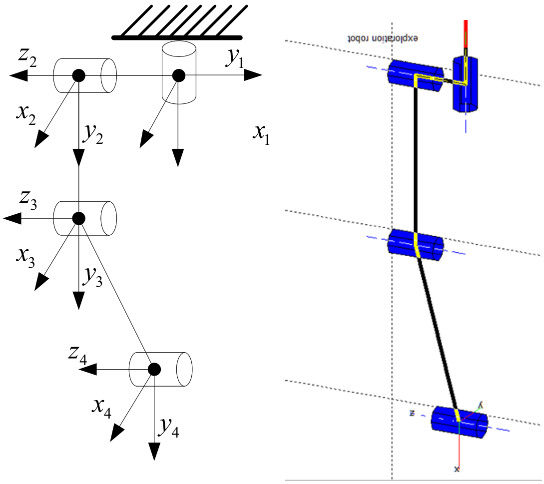

Figure 3. D-H robotic arm link coordinate system

The Newton-Euler recursive method is employed to derive the dynamics of the robotic arm. The motion control simulation platform for the robotic arm in this paper utilizes Matlab combined with the Robotic Toolbox. The Robotic Toolbox supports the standard Matlab programming environment and boasts powerful graphical display capabilities, enabling the creation of robot link models. It is widely used by researchers in the field of robotics. This paper's research is based on some fundamental modeling rules provided by this toolbox. Based on the actual parameters of the dual-arm robot developed, a simulation model consistent with the actual robot body parameters is established. The D-H coordinate distribution is illustrated in Figure 3.

Calculate the driving torque and inertia change of each joint using the equation.

$$H(\theta)\ddot{\theta}+C(\theta,\dot{\theta})\dot{q}+G(\theta)=\tau \tag{1}$$

In the formula θ, $\dot{\theta}$, and $\ddot{\theta}$ represent the joint angle, velocity, and acceleration of the robotic arm, respectively. $H(q)\ddot{q}$ represents the inertial force proportional to the generalized acceleration $\ddot{\theta}$. Each component in $C(\theta,\dot{\theta})\dot{\theta}=\left[\dot{\theta}^T C_1\dot{\theta} \;\ldots\; \dot{\theta}^T C_n\dot{\theta}\right]^T$ is a quadratic form of the generalized velocity. $G(\theta)$ represents the gravity term, and τ represents the theoretical driving torque output by each joint. Proportional-derivative (PD) robotic arm controllers are designed in joint space and Cartesian space, as shown in Figures 4 and 5. The inertia change e, joint torque τ , joint angle, and velocity θ, $\dot{\theta}$ can be configured and selected as system inputs.

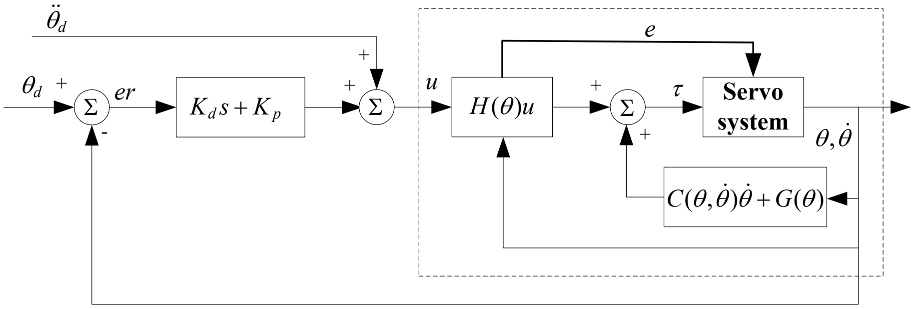

Figure 4. D-H robotic arm link coordinate system

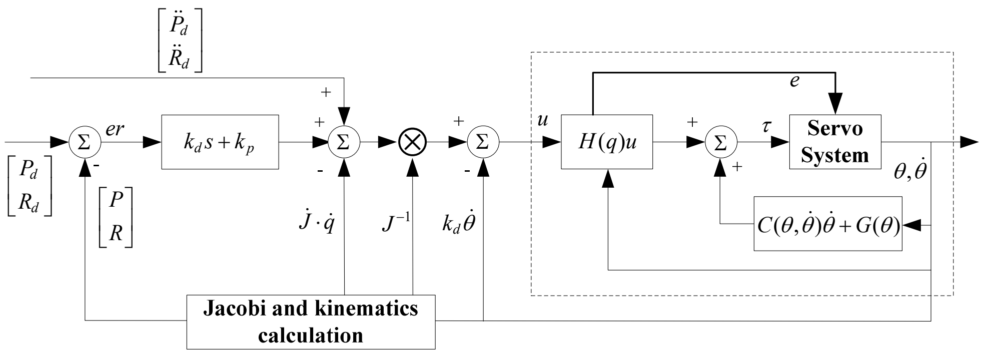

Figure 5. D-H robotic arm link coordinate system

In this way, through dynamic calculations of the robotic arm, the rotational inertia of each joint in the robot dynamics can be obtained periodically in real-time, and the calculated joint angles can be used as input variables for the fuzzy controller.

4. Intelligent Joint Fuzzy PID Control Strategy

4.1. The Idea of Fuzzy Controller

The speed loop controller is a traditional proportional-integral (PI) controller. Its performance has been optimized to the limit, and the author has also made significant improvements in details such as the joint tuning of position, speed, and current loops, as well as saturation suppression.

As shown in Figure 2, the robot is a four-joint series system. Its posture changes with the control commands from the host computer, resulting in a constantly changing moment of inertia and torque. Due to this characteristic of variable moment of inertia and torque, traditional PI regulators cannot effectively control speed fluctuations, which in turn can cause vibrations in the robot. Therefore, this paper designs a fuzzy PID controller to act on the speed loop [8].

As shown in Figure 6, a two-dimensional fuzzy controller is added to the traditional speed loop PID control. The change in rotational inertia e and the rate of change of rotational inertia deviation ec are selected as the inputs to the fuzzy controller. The fuzzy inference link infers and outputs them based on the deviation and the rate of change of deviation to correct the proportional, integral, and derivative parameters of the PID regulator. These parameters are then applied to the PID regulator, continuously correcting the parameters of the PID controller online in real time, so that the system ultimately outputs satisfactory control effects. The fuzzy control rules are naturally formed in this process. The final PID control parameters of the speed loop can be expressed as:

$$\begin{cases} k_p = k_p^{'} + \Delta k_p \\ k_i = k_i^{'} + \Delta k_i \\ k_d = k_d^{'} + \Delta k_d \end{cases} \tag{2}$$

In the formula, $k_p^{'}$, $k_i^{'}$, and $k_d^{'}$ represent the initial values of the system's PID controller, which are obtained through conventional PID tuning methods. Δk_p, Δk_i, and Δk_d represent the output values of the fuzzy controller, and the values of the three control parameters are automatically adjusted based on the robot's posture [9].

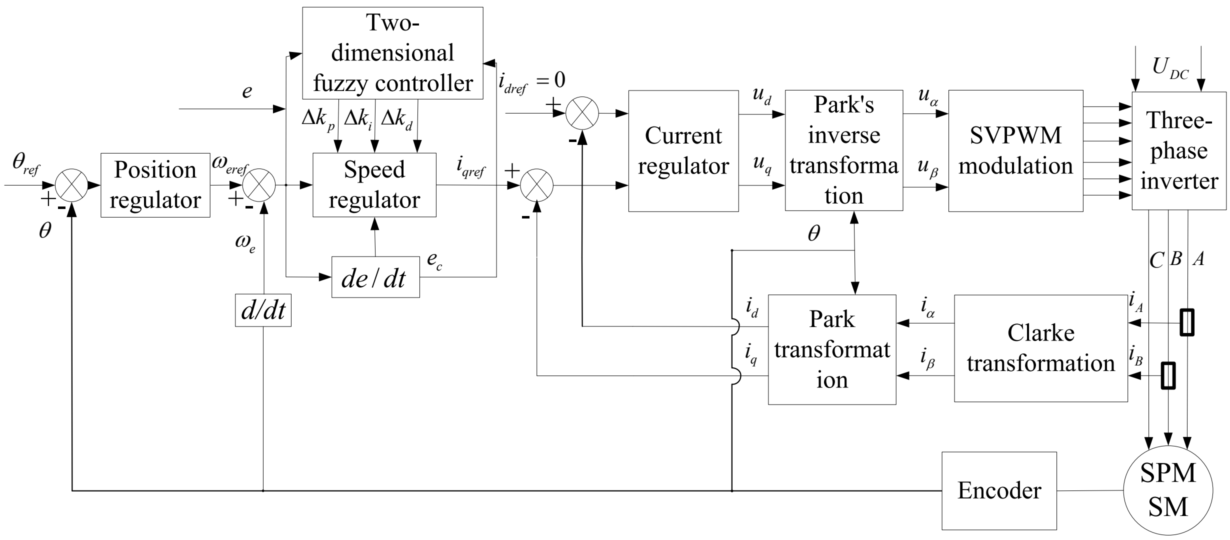

Figure 6. D-H robotic arm link coordinate system

4.2. Fuzzy Controller Design

The joint with the largest change in robotic rotational inertia is the second joint, so the second joint is taken as an example to design the fuzzy controller.

(1) Determine the input and control variables

The input variables are the change e and the rate of change ec of the rotational inertia J of the robotic arm. Corresponding to the domain of discourse

$e = \{-6,-5,-4,-3,-2,-1,0,1,2,3,4,5,6\}$

$ec = \{-3,-2,-1,0,1,2,3\}$

Select fuzzy subsets e、ec

e、$ec = \{NB, NM, NS, ZE, PS, PM, PB\}$

The control variables are the proportional, integral, and derivative changes Δk_p, Δk_i, and Δk_d. For speed loop PID control, the derivative control variable is generally zero. Therefore, only fuzzy calculations need to be performed on Δk_p and Δk_i. Select the domain

$\Delta k_p = \{-6,-5,-4,-3,-2,-1,0,1,2,3,4,5,6\}$

$\Delta k_i = \{-3,-2,-1,0,1,2,3\}$

Select fuzzy subsets Δk_p and Δk_i

Δk_p、$\Delta k_i = \{NB, NM, NS, ZE, PS, PM, PB\}$ The corresponding scope of the domain: $\Delta k_p = [-0.8, 0.8]$, $\Delta k_i = [-0.03, 0.03]$.

(2) Establishment of membership function

Common membership functions include triangular membership function, Sigmoid membership function, and bell-shaped membership function. Based on the characteristics and experience of intelligent joint control, the triangular membership function is selected as follows:

$$u_{(x)} = \begin{cases} 0, x \le a \\ \dfrac{x-a}{b-a}, a \le x \le b \\ \dfrac{c-x}{c-b}, b \le x \le c \\ 0, c \le x \end{cases} \tag{3}$$

Figure 7 depicts the curve of the triangular membership function. In this paper, the curves e, ec, Δk_p, and Δk_i all follow an isosceles triangle distribution.

4.3. Establishment of Fuzzy Control Rule Base

Fuzzy control rules are the core of fuzzy controllers, and there are generally two methods for their generation: one is to summarize and deduce them based on the practical experience and knowledge of operators or experts in controlling the system; the other is to test and experiment with the system, and summarize and deduce them from the analysis of the system's input and output data.

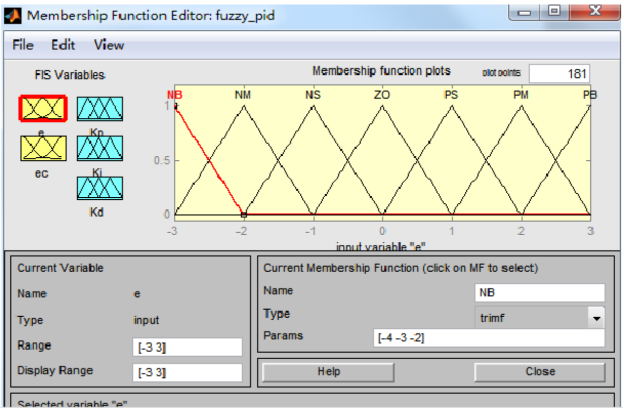

Figure 7. Triangular membership function curve

In robot applications, rotational inertia needs to be introduced to establish the rule table. However, calculating rotational inertia is a very complex process. For the controller, the robot's real-time pose is known. Based on the aforementioned robot spatial dynamics model, the rotational inertia of the robot can be calculated. The real-time rotational inertia can be transmitted to the speed loop controller through the robot's EtherCAT bus [10].

For Δk_p and Δk_i , each has 7*7=49 control rules, thus establishing a control rule table.

Figure 8. PI parameter tuning experimental device for variable moment of inertia

Experience data was obtained through pendulum experiments with different rotational inertia. As shown in Figure 8, a single-arm test platform was built to simulate the load of a Scara robot. By simply replacing different weights at the end, the rotational inertia of the load could be changed. The parameters of the speed loop PI controller were manually adjusted to achieve optimal output under different rotational inertia, thereby establishing fuzzy control rules.

(1) When e is positive and ec is positive, select a positive Δk_p value and a negative Δk_i value.

(2) When e is positive and ec is in the middle, select the positive Δk_p value and the negative Δk_i value.

Table 3. Control rule table of Δk_p

Δk_p Ec e	NB	NM	NS	ZE	PS	PM	PB
NB	NB	NB	NM	NM	NS	ZE	ZE
NM	NB	NB	NM	NS	NS	ZE	ZE
NS	NB	NM	NS	NS	ZE	PS	PS
ZE	NM	NM	NS	ZE	PS	PM	PM
PS	NM	NS	ZE	PS	PS	PM	PB
PM	ZE	ZE	PS	PS	PM	PB	PB
PB	ZE	ZE	PS	PM	PM	PB	PB

Table 4. Control rule table of Δk_i

Δk_i ec e	NB	NM	NS	ZE	PS	PM	PB
NB	PB	PB	PM	PM	PS	ZE	ZE
NM	PB	PB	PM	PS	PS	ZE	ZE
NS	PB	PM	PS	PS	ZE	NS	NS
ZE	PM	PM	PS	ZE	NS	NM	NM
PS	PS	PS	ZE	NS	NS	NM	NB
PM	ZE	ZE	NS	NS	NM	NB	NB
PB	ZE	ZE	NS	NM	NM	NB	NB

4.4. Fuzzy Reasoning and Defuzzification

After establishing the fuzzy rule table, the corresponding values of Δk_p and Δk_i can be obtained based on the changes in load moment of inertia, that is, the changes in e and ec . For robots with variable posture and variable moment of inertia, the change amount and change rate of moment of inertia can be obtained according to the aforementioned robot dynamics model.

After obtaining the actual value of the rotational inertia change at the load end, values Δk_p and Δk_i are calculated based on the fuzzy rule table, and fuzzy operation is performed. In this paper, the Mamdina rule is adopted for fuzzy inference. For the data after fuzzy inference, it is necessary to perform fuzzy clarification processing. Common strategies for defuzzification include the maximum membership method, the centroid method, and the median method. This paper adopts the centroid method.

For the input vector and the vectors $u_c^*(i)$ and $C^*(i)$ obtained after fuzzy inference, the formula for the discrete centroid method is:

$$f = \frac{\sum_{i=1}^{p} c^*(i) u^*_c(i)}{\sum_{i=1}^{p} u^*_c(i)} \tag{4}$$

In the formula, p represents the number of elements in vector $C^*(i)$.

5. Experiment and Analysis

The experimental results utilize the EtherCat communication bus to export real-time motor speed waveform and current waveform data, and to generate graphs, with a communication sampling period of 1ms. The servo driver employs position control in EtherCat communication mode, selecting two-axis intelligent joints for result analysis. A green harmonic LHSG-20-100-C-I-S540 reducer is installed on the motor output shaft, with a reduction ratio of 1:101. The motor has a rated speed of 3000 rpm and a rated current of 2.4A. The position feedback loop employs dual encoders for measurement to obtain the absolute position of the motor. The motor end uses an incremental encoder to obtain the position per revolution, while the harmonic reducer end uses a Renishaw magnetic encoder to obtain the multi-turn position of the motor. The given joint low-speed end output position is ±180 degrees. The maximum operating speed of the servo motor is 2000 rpm/min. Under these experimental conditions, current waveforms under a traditional PI controller and a fuzzy adaptive PI controller are collected for comparative analysis.

As shown in Figure 9, the blue curve represents the speed reference, while the red curve represents the speed feedback. When the reducer oscillates back and forth through a range of ±180 degrees, the motor speed increases from 0 to 2000 rpm, then decelerates to 0 rpm, reverses direction and accelerates to -2000 rpm, and finally slows down to 0. This represents the position loop's repetitive positioning control of a servo driver.

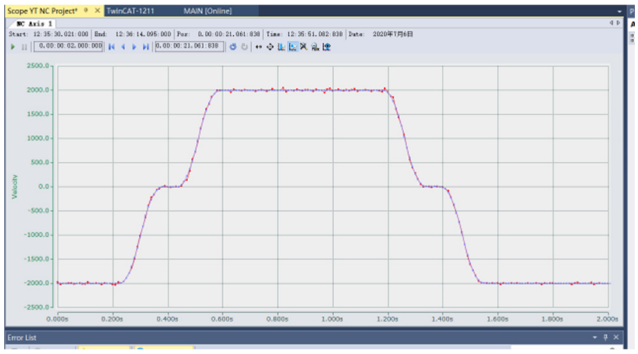

Figure 9. Speed fluctuation of traditional PI controller

As can be seen from Figure 10, under the given condition of a speed of 2000 rpm, the speed fluctuation range of the traditional PI controller reaches ±30 rpm, and it is an equal-amplitude oscillation.

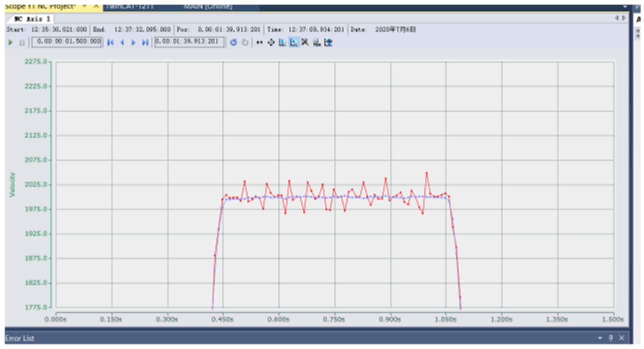

Figure 10. Local magnified diagram of speed fluctuation

As shown in Figure 11, the blue line represents the given current waveform of the traditional PI controller, while the red line represents the actual current waveform. During the acceleration phase, the peak output current is 3A. When operating at a steady state of 2000 rpm, the peak-to-peak current fluctuation ranges from -0.8 to 1.4, with a total current fluctuation of 2.2A.

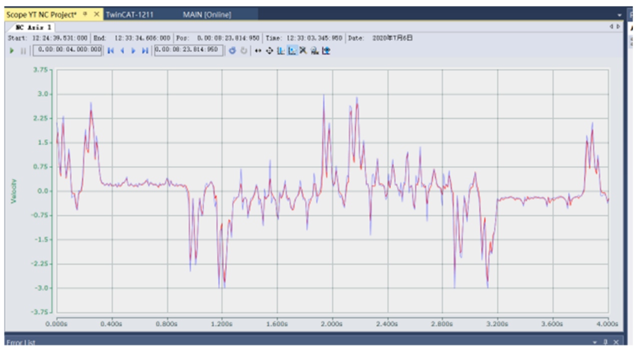

Figure 11. Current following curve

As shown in Figure 12, when the speed reaches 2000 rpm, the speed fluctuation of the fuzzy PI controller quickly converges, with the converged speed fluctuation being ±12 rpm, whereas the speed fluctuation of the traditional PI controller is ±30 rpm.

As shown in Figure 13, the current fluctuation of the fuzzy controller at a steady-state speed of 2000 rpm is around 0.5A, and at a speed of -2000 rpm, the current fluctuation is 0.8A. The forward and reverse speed fluctuations are much smaller than those of the traditional PI controller.

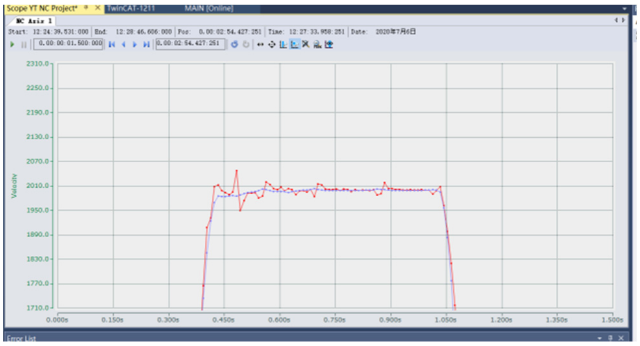

Figure 12. Speed waveform of fuzzy adaptive PI controller

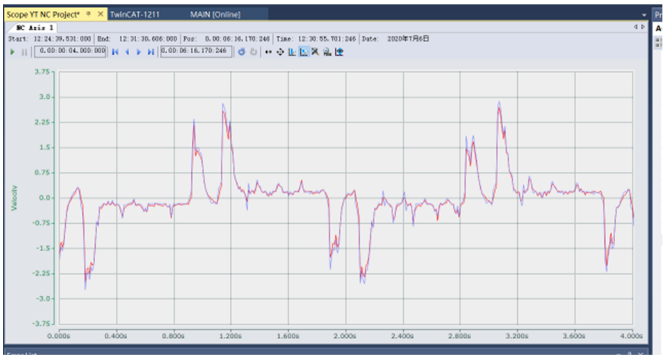

Figure 13. Current waveform of fuzzy adaptive PI controller

6. Conclusion

This article conducts research on vibration suppression for underground power grid inspection robots. By employing a fuzzy control strategy, it calculates the moment of inertia and its rate of change in real-time to establish fuzzy rules. Additionally, it redesigns the speed loop controller to manage rotational speed fluctuations of the robot. Through comparative analysis of experimental data, it is found that using a fuzzy adaptive PI controller, which automatically adjusts the output of the PI controller based on different moment of inertia of the robot, achieves significant results. Satisfactory outcomes have been obtained in both speed fluctuation and current fluctuation aspects. Future work involves further optimizing control rules, reducing the speed overshoot of the fuzzy controller, and further minimizing current fluctuations.

Acknowledgments

The authors thank the editor and anonymous reviewers for their valuable remarks and helpful suggestions. This study was partially supported by the Provincial Research Platform Opening Fund of Yancheng Polytechnic College (YGKF202201).

References

[1] Sun, L F; Liang, F Y and Fang, L J. "Chatter Vibration Analysis of A Novel Industrial Robot for Robotic Boring Process", IEEE International Conference on Intelligence and Safety for Robotics (ISR), 2018, pp.56-6.

[2] Kim, J and Croft, E A, "Preshaping input trajectories of industrial robots for vibration suppression", Robotics and Computer-Integrated Manufacturing, 2018, 54, pp.35-44.

[3] Elvira-Ortiz, D A; Romero-Troncoso, Osornio-Rios, R A et al. "Vibration Suppression for Improving the Estimation of Kinematic Parameters on Industrial Robots ", Shock and Vibration, 2016.

[4] Wang M, Liu X, Dong X, et al. A novel method to detect and suppress mechanical resonance for servo system[C]//2016 9th International Symposium on Computational Intelligence and Design (ISCID). Hangzhou, China, 2016, 1: 349-354.

[5] Chen Y, Yang M, Sun Y, et al. A Modified Bi-Quad Filter Tuning Strategy for Mechanical Resonance Suppression in Industrial Servo Drive Systems[J]. IEEE Transactions on Power Electronics, 2021, 36(9): 10395-10408.

[6] Yang S M, Wang S C. The detection of resonance frequency in motion control systems[J]. IEEE Transactions on Industry Applications, 2014, 50(5): 3423-3427.

[7] Chen J. Research on neural network energy-efficient control technology in robot systems[D]. Xidian University, 2015.

[8] Su X H. Design of PID controller based on fuzzy control theory[J]. Management informatization in China, 2019, 22(3): 136-139.

[9] Wang A, Yang Q Q, Run W Y. Design and simulation of fuzzy self-tuning PID controller[J]. Computer Simulation, 2012, 29(12): 224-228.

[10] Wang C, Yang M, Xu D G. Suppression of mechanical resonance in a dual-inertia elastic system based on PI control[J]. Electric Drive, 2015, 45(1).